Proceedings of the ASME 2018 37th International Conference on Ocean, Offshore and Arctic Engineering
OMAE2018
June 17-22, 2018, Madrid, Spain

OMAE2018-78315

HYDRODYNAMIC COEFFICIENTS OF SIMPLIFIED SUBSEA STRUCTURES

Fredrik Mentzoni*
Mia Abrahamsen-Prsic
Trygve Kristiansen
Department of Marine Technology
Norwegian University of Science and Technology
NO-7491 Trondheim, Norway

ABSTRACT

Simplified two-dimensional models, representing components of complex subsea structures, are experimentally investigated. Individual as well as combinations of components in different configurations are tested, in order to study the effect of hydrodynamic interaction. The components include porous plates and cylindrical pipes with circular cross-section. Hydrodynamic added mass and damping coefficients, relevant for force estimation during lifting operations, are presented. The coefficients are obtained based on forced oscillation tests for a large range of Keulegan–Carpenter (KC) numbers and forcing periods, and compared to numerical source panel results for the low KC limit, as well as recommendations given by DNV GL, where relevant.

Coefficients for all configurations are found to be highly amplitude dependent. Significant interaction effects are found for the assembled structures, causing either reduced or increased total added mass and damping coefficients compared to the superposition of the coefficients for individual members.

NOMENCLATURE

A Hydrodynamic added mass coefficient [kg]
A_0 Hydrodynamic added mass of a solid plate [kg]
B Hydrodynamic damping coefficient [kg/s]
B_1 Linear damping coefficient [kg/s]
B_2 Quadratic damping coefficient [kg/m]
D Characteristic length – width or diameter [m]
F Measured net force [N]
M Mass [kg]
P Porosity ratio in percent [%]
p Porosity ratio [–]
R Radius of cylinders [m]
T Oscillation period [s]
W Vertical velocity amplitude [m/s]
w_l Equivalent velocity [m/s]
Z Amplitude of motion [m]
β Ratio of Reynolds to Keulegan–Carpenter number [–]
η Vertical position [m]
$\dot{\eta}$ Vertical velocity [m/s]
$\ddot{\eta}$ Vertical acceleration [m/s^2]
μ Discharge coefficient [–]
ν Kinematic viscosity [m^2/s]
ρ Density [kg/m^3]
ω Circular oscillation frequency [1/s]
KC Keulegan–Carpenter number [–]
KC_{por} Porous Keulegan–Carpenter number [–]
Re Reynolds number [–]

INTRODUCTION

Marine operations involving lifting and lowering of subsea modules from a ship deck to the sea bottom, or vice versa, have operational restrictions related to environmental conditions such as waves, wind and current. The hydrodynamic loads on the

*Corresponding author: fredrik.mentzoni@ntnu.no

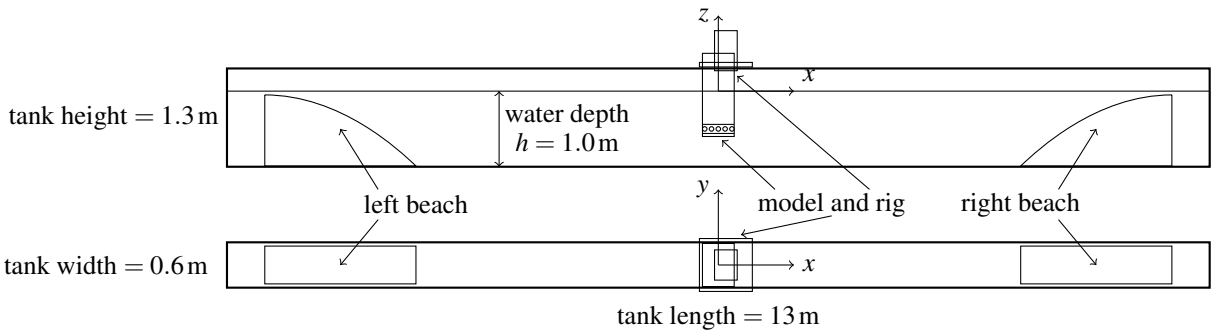

FIGURE 1. SKETCH OF THE TANK. UPPER: SIDE VIEW. LOWER: BIRD'S EYE VIEW.

structures as they are lifted and lowered, are, in general, important for the crane hook load, one of the key limitations of such operations.

As subsea field developments are getting more extensive, with increasing demand for operability, the need for performing all-year operations is increasing. All-year operations imply an increasing risk of harsh conditions. Without proper estimates of the expected hydrodynamic loads, this can lead to overcompensation of required vessel and crane capabilities, costly delays, and – at worst – unsafe operations with risk for equipment and personnel. Proper load estimates are the key for planning and simulation training in order to give a realistic description of the operation. Hence, in order to be able to perform safe and cost-efficient marine operations all-year, there is a need for careful assessments of the hydrodynamic loads on subsea structures, including hydrodynamic added mass and damping coefficients for typical members of subsea modules and their interaction.

Configurations of cylinder elements and porous plates have been experimentally investigated in a glass wall wave flume at the Norwegian University of Science and Technology (NTNU). The configurations mimic characteristics of actual subsea modules that typically consists of equipment and protection structures with similarities to porous plates and cylinder elements. Special attention has been given to the interaction effects between different members of the modules. A description of the experimental setup, the different configurations, the hydrodynamic coefficients, and results are given in the following sections.

EXPERIMENTAL SETUP

The tests are performed in a wave flume at the Marine Technology Center in Trondheim. A sketch of the tank is given in Fig. 1. The tank is 13 m long and 0.60 m wide. A near two-dimensional setup is used. The water depth is 1.0 m in all tests. Parabolic beaches are placed on both sides of the tank to avoid wave reflections. The rig is placed in the middle of the tank, 6.5 m from each side.

The oscillating rig consists of two acrylic glass plates, fastened to a wooden box on the top end, that is connected to a steel frame and actuator on the top, see Fig. 2. The distance between the acrylic plates and the glass walls of the tank was approximately 9 mm. The actuator acts in the vertical direction along a rail supported threaded drive shaft that is connected to an electrical motor through a belt drive. The force on the entire rig is measured by a 400 N force transducer located in the intersection between the model rig and the actuator. Motions of the models are monitored by six accelerometers attached to the rig, while the free-surface elevation is measured by six wave probes at different locations between the rig and the beaches. All measurements are recorded at a sample rate of 200 Hz with Butterworth filtering at 20 Hz. Further, the measurements are band-pass filtered around the basic harmonic of the oscillation when calculating the hydrodynamic coefficients and wave elevations.

Forced oscillation sinusoidal sequences are used as input signal for the electrical motor that actuates the configurations vertically. The signal is read by the actuator at a sample rate of 50 Hz. The test sequences consist of harmonically varying signals, with a given amplitude, and period, of oscillation. Each sequence consist of 20 periods of oscillations. The first five and the last five periods are used to ramp the signal gradually from/to zero to/from the prescribed amplitude of motion. The tested periods of oscillations, with corresponding markers used in the result figures, are as follows: 1.0 s (diamonds), 1.25 s (pentagons), 1.5 s (hexagons), 1.75 s (circles), and 2.0 s (stars).

MODEL CONFIGURATIONS

The four tested configurations are presented in Table 1. All configurations consist of 570 mm long (in the y-direction, Fig. 1) aluminum plates and/or cylinder members fastened to the two acrylic plates. The configurations are all installed as close to mid-water as possible. The average distance from the center of each configuration to the tank bottom and free surface is thus approximately 0.5 m.

TABLE 1. EXPERIMENTAL CONFIGURATIONS

Config.	Structures	Mass
1	1 porous plate	2.1 kg
2	5 cylinders	7.4 kg
3	2 porous plates	4.2 kg
4	2 porous plates and 5 cylinders	11.6 kg

Configuration 1 is a single porous plate consisting of many equally distant circular holes of 3 mm diameter with 2 mm distance between the outer edge of each hole. The plate is 420 mm wide (x-direction in Fig. 1), 3 mm thick and has a mass of 2.1 kg. Two 20 mm wide aluminum fittings are fastened along the length span (y-direction) of the plates, 9 cm from each plate end, to provide stiffness against bending. These stiffeners are not perforated. In order to fasten the porous plate to the end plates, two (partly perforated) aluminum profiles, screwed onto the ends of the plates, are used, see Fig. 3. The porosity of the plate is $P = 27.8\,\%$ when accounting for the stiffeners and the fastening profiles.

Configuration 2 consists of five circular cylinders, with radius $R = 30$ mm and mass $1.47\,\text{kg} \pm 0.03\,\text{kg}$, placed in a row. The cylinders are fastened with a wall-to-wall distance of 30 mm. The total width of the configuration is hence 420 mm, the same as the porous plate, and an equivalent porosity for the configuration as a whole is $\frac{4R}{14R} = 28.6\,\%$. The cylinders are filled with a PVC based material, in order to prevent water from flowing inside the cylinders.

Configuration 3 consists of two porous plates of the same type as in configuration 1. The two porous plates are placed in parallel with 120 mm vertical distance from each other.

In configuration 4, shown in Fig. 3, the five cylinders of configuration 2 are placed between the two parallel plates of 120 mm distance (config. 3), in the exact same manner as in configuration 2. Abbreviated names used in figures are thus 1 pp, 5 cyl, 2 pp, and 2 pp + 5 cyl, for configurations 1–4 respectively, with pp and cyl being abbreviations for porous plate(s) and cylinders. In plots where the results for one porous plate are doubled for comparison with the two parallel plates, the abbreviated legend name 2×1 pp is used.

HYDRODYNAMIC COEFFICIENTS

The experimental results are presented in terms of hydrodynamic coefficients and will be discussed through dependency on the Keulegan–Carpenter number, KC, and the oscillation period, T. Hydrodynamic added mass and damping coefficients are calculated based on the measured vertical force and acceleration.

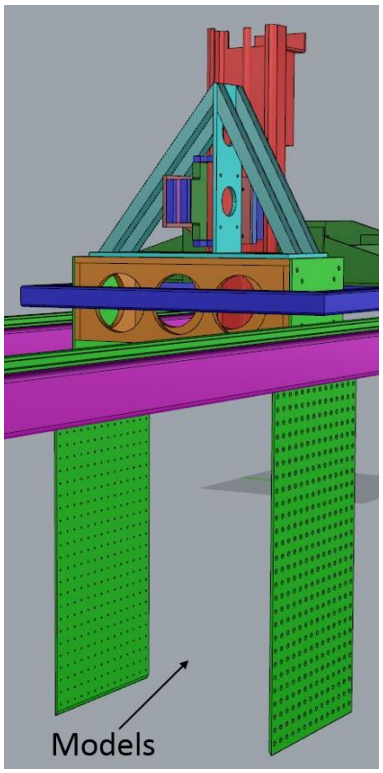

FIGURE 2. SKETCH OF THE MODEL RIG SHOWING ACRYLIC GLASS PLATES (GREEN), WOODEN BOX (ORANGE), STEEL FRAME (CYAN) AND MOTOR CONNECTION (RED).

The measured force in tests without model, with rig only, is subtracted time-step by time-step, in order to obtain the net force on a configuration. Assuming a linear damping model, Newton's 2nd law yields

$$(M+A)\ddot{\eta} + B\dot{\eta} = F, \tag{1}$$

with M being the dry mass of the model, A the added mass coefficient, $\ddot{\eta}$ the acceleration, B the damping coefficient, $\dot{\eta}$ the velocity and F the measured net force. Since the motions are harmonically varying, the added mass and damping coefficients are obtained by Fourier averaging,

$$(M+A)\int_{nT} \ddot{\eta}\,\ddot{\eta}\; dt + 0 = \int_{nT} F\,\ddot{\eta}\; dt, \tag{2}$$

$$0 + B\int_{nT} \dot{\eta}\,\dot{\eta}\; dt = \int_{nT} F\,\dot{\eta}\; dt, \tag{3}$$

where the integrations are performed over an integer number, n, periods of oscillations, T. Here, all quantities are band-pass fil-

tered around the basic forcing harmonic. The presented results are based on the mean of the coefficients for eight of the ten steady-state forcing periods, avoiding the first and last forcing periods as well as the ramp in and out.

The force coefficients are typically functions of the Reynolds number,

$$\mathrm{Re} = \frac{WD}{\nu}, \tag{4}$$

relating the forced vertical velocity magnitude, W, times the characteristic length, D, to the kinematic viscosity, ν, as well as the KC number,

$$\mathrm{KC} = \frac{WT}{D}, \tag{5}$$

which relates the velocity magnitude, W, to the period of oscillations, T, and the characteristic length, D. The ratio of these two dimensionless quantities is recognized as the β value,

$$\beta = \frac{\mathrm{Re}}{\mathrm{KC}} = \frac{D^2}{\nu T}. \tag{6}$$

For harmonic motions, the KC number simplifies to

$$\mathrm{KC} = 2\pi\frac{Z}{D}, \tag{7}$$

with Z being the amplitude of the harmonic motion. For porous structures, the KC number can be modified to account for the pressure drop and the force caused by the flow through the perforations,

$$\mathrm{KC}_{\mathrm{por}} = \mathrm{KC}\frac{1-p}{4\pi\mu p^2} = \frac{Z}{D}\frac{1-p}{2\mu p^2}, \tag{8}$$

with μ being a dimensionless discharge coefficient and p being the porosity ratio [1]. Hence, when plotting against $\mu\mathrm{KC}_{\mathrm{por}}$, a reduction of the spread between results for different porosities is expected [2].

The tested amplitudes of motions range from 16 mm to 166 mm, corresponding to KC numbers from 0.25 to 2.5 for a characteristic length equal to the width of the tested porous plates, $D = 420$ mm. When the porosity is $P = 27.8\,\%$, the corresponding porous KC number range is $0.18 \leq \mu\mathrm{KC}_{\mathrm{por}} \leq 1.8$. For a full size module with a characteristic length of 10 m, the range of KC numbers corresponds to wave amplitudes from 0.4 m to 4.0 m, and the tested periods of oscillation, $1.0\,\mathrm{s} \leq T \leq 2.0\,\mathrm{s}$, correspond to wave periods from 4.9 s to 9.8 s.

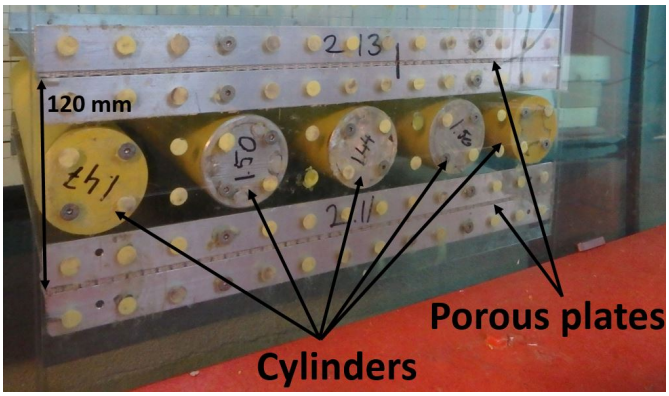

FIGURE 3. CONFIGURATION 4 CONSISTING OF TWO POROUS PLATES AND FIVE CYLINDERS.

In addition to figures with $\mu\mathrm{KC}_{\mathrm{por}}$ on the horizontal axis, damping is presented as function of the equivalent velocity obtained with the method of equivalent linearization [3, p. 98],

$$B\dot{\eta} = \left(B_1 + B_2\frac{16}{3}\frac{Z}{T}\right)\dot{\eta}, \tag{9}$$

where

$$w_l = \frac{16}{3}\frac{Z}{T} \tag{10}$$

is recognized as the equivalent velocity. B_2 is a representation of the quadratic damping contribution.

The infinite fluid added mass of a solid plate with width D and length L, as predicted by potential flow theory,

$$A_0 = \rho\frac{\pi}{4}D^2L, \tag{11}$$

is, in general, used to normalize the coefficients. To provide the dimensionless damping coefficients, normalization with the solid plate added mass, A_0, times the circular frequency, ω, is used.

COMPARISON AND VERIFICATION

The model test results are compared with different methods of estimation and previous experimental results where relevant. Added mass coefficients for $\mathrm{KC} \to 0$ are obtained using a numerical potential flow solver, a two-dimensional boundary element method (BEM) developed within the present work. The added mass results are also compared with the recommended practice by DNV GL [4], which is widely used by the industry [5]. Further, the single porous plate test is compared with the

TABLE 2. ADDED MASS NORMALIZED WITH ONE SOLID PLATE BASED ON RECOMMENDATIONS IN DNVGL-RP-N103

Config.	Low KC, Eq. (12)	All KC, Eq. (13)
1	0.37	0.54
2	0.10	0.10
3	0.74	1.09
4	0.84	1.20

experimental results for a realistic three-dimensional model of an actual protection roof structure [2, 6]. This protection structure model consists of several parallel cylinders and has an equivalent porosity of $P = 26.7\,\%$ [2, 6].

The BEM results are obtained using a two-dimensional, lowest order (constant strength) source panel method. The results are checked for numerical convergence, and the code was first verified against analytical solutions for the added mass of simpler structures. Each member of a structure is modeled using 100 elements. Ideal porous plates, where the number of openings goes to infinity, will have zero added mass at zero amplitude [1]. Consequently, only the non-perforated aluminum stiffeners are included in the BEM models of the porous plates. To account for the partly perforated fastening profiles, the stiffeners are made 20 mm larger in the BEM models than their actual size in the experiments.

DNVGL-RP-N103 [4] is a recommended practice (RP) for modeling and analysis of marine operations. There are two estimates for the added mass of porous structures in the RP. In Section 3.3.4.4, a relation based on a curve fit of results for plates with circular holes, is given for the added mass of porous structures at the low KC limit,

$$\left.\frac{A}{A_0}\right|_{KC\to 0} = \exp^{\left(-\frac{p}{0.28}\right)}, \tag{12}$$

with p being the porosity ratio of the plate and A_0 is given by Eq. (11). An alternative empirical relation expressing the effect of perforation on the added mass, based on model test data, including a safety margin, is given in Section 4.6.4.1 of the RP,

$$\frac{A}{A_0} = 0.7 + 0.3\cos\left(\frac{\pi(P-5)}{34}\right), \quad 5 < P < 34, \tag{13}$$

with P being the porosity of the plate in percentage.

A list of the estimated added mass using Eqs. (12) and (13) for the tested configurations, is given in Table 2. The added mass of the cylinders are here estimated based on the superposition of five times the added mass of one cylinder, which is provided in App. A of the RP [4], and given by Eq. (11) when $D = 2R$ is the diameter of the cylinder. All values are normalized with the added mass of one solid plate with the same dimensions as the tested porous plates.

RESULTS

Experimental results for the four different configurations are presented in this section. The results are split in subsections. In the first subsection, the experimental results from the simple structures, the single plate (config. 1) and five in-line cylinders (config. 2), are presented. In the following subsections, the parallel plates (config. 3) is first compared with two times the single plate results, then with the assembled configuration consisting of two parallel plates with five cylinders in between (config. 4). A comparison of the relative importance of the damping force compared to the added mass force, is then given. We emphasize that the damping force in general dominates over the added mass force. Lastly, the damping coefficients of the four configurations are presented as functions of the equivalent velocity. Our results indicate that this commonly used model gives a rather modest representation of the forces.

Single plate and in-line cylinders

Added mass and damping results for configurations 1 and 2 of, respectively, 1 porous plate (1 pp) and 5 cylinders (5 cyl), are presented in Figs. 4 and 5. The previously published experimental results of a realistic model of an actual subsea protection structure [2, 6], are represented by black markers in the figures. Left-pointing triangles are used for their results at a (full scale) forcing period of $T = 6\,$s, whereas right-pointing triangles represent $T = 10\,$s. Being a three-dimensional investigation, their results are made dimensionless based on the three-dimensional solid added mass as provided in their study [2, 6].

The dimensionless added mass coefficients are plotted against $\mu\mathrm{KC}_{\mathrm{por}}$ in Fig. 4, where the characteristic length is the width of the plate, $D = 420\,$mm, and the equivalent porosity $P = \frac{4R}{14R} = 28.6\,\%$ is used for the cylinder configuration, while the plate porosity is $P = 27.8\,\%$. The standard deviation based on the eight steady-state forcing periods (neglecting the first and last as well as the ramp in and out) used to calculate the mean coefficients, is illustrated with error bars in the figure. All tested configurations yield quite small standard deviations (for both added mass and damping), typically 1–3 % of the mean value. To increase readability, error bars are therefore left out in the remaining figures.

The added mass of both configurations are found to be highly amplitude dependent. The five cylinders case has a significant added mass at small amplitudes of motion, and in general

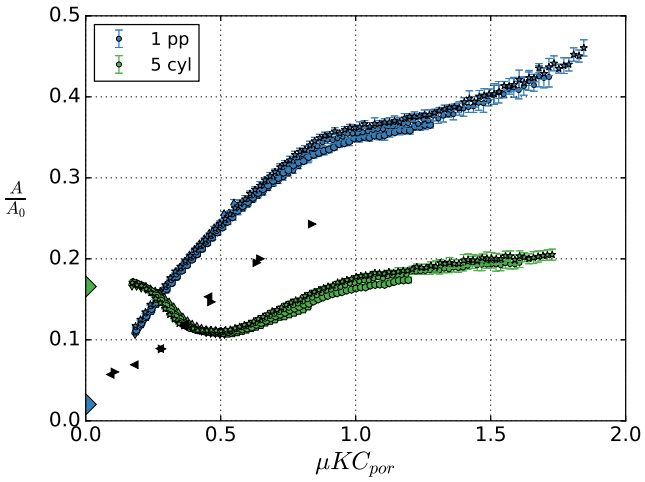

FIGURE 4. ADDED MASS OF A POROUS PLATE AND FIVE IN-LINE CYLINDERS. BLACK MARKERS ARE RESULTS FOR A SUBSEA PROTECTION STRUCTURE [2, 6]. BEM RESULTS ARE ILLUSTRATED BY THE MARKERS AT ZERO AMPLITUDE.

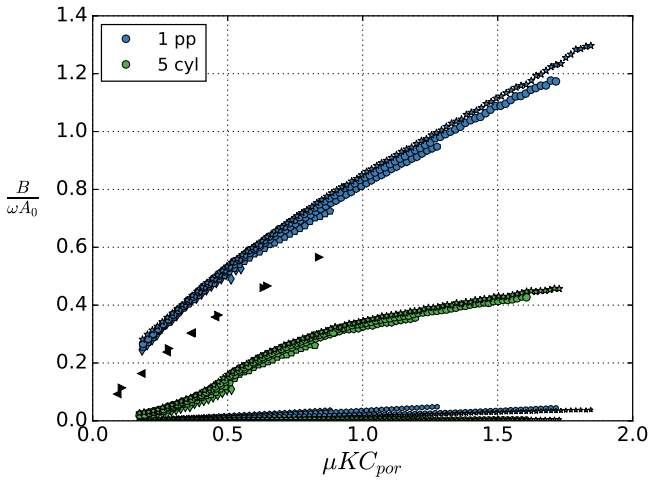

FIGURE 5. MEASURED DAMPING AND ESTIMATED WAVE RADIATION DAMPING OF A POROUS PLATE AND FIVE IN-LINE CYLINDERS. BLACK MARKERS ARE RESULTS FOR A SUBSEA PROTECTION STRUCTURE [2, 6].

less variation with amplitude compared to the porous plate. For the porous plate, slight variations in amplitude yield significant changes in the added mass coefficient, which experiences a rapid increase from 0.11 to 0.46 for $\mu\mathrm{KC}_{\mathrm{por}}$ in the tested range. For both configurations, the potential flow solver yields added mass coefficients that are in reasonable agreement when extrapolating the experimental results towards zero amplitude of motion. The expected values will depend on the extrapolation technique. If, for instance, the expected value is based on linear extrapolation from the three smallest amplitudes from the five forcing periods, the relative differences between the expected value and the BEM result are 16 % and 13 % for, respectively, config. 1 and 2, when using the expected value as reference value. The potential flow solver result obtained for the five cylinders yields an added mass coefficient equivalent to 1.62 times the added mass of five cylinders superposed, that is, a 62 % increase in added mass due to potential flow interaction between the five cylinders. Consequently, the added mass of the configuration is underestimated if using superposition of added mass of one cylinder as in Table 2. Contrary, the relations for the added mass of porous structures in DNVGL-RP-N103 are found to be conservative compared to the experimental results. The low KC relation in Eq. (12) yields $\frac{A}{A_0} = 0.37$, which is a good estimate for the highest amplitudes, while the more conservative Eq. (13) results in $\frac{A}{A_0} = 0.54$, somewhat above the experimental values even for the highest amplitudes tested.

The added mass coefficient of the five cylinders (config. 2) follows a behavior that share similarities with previous results for one cylinder. In particular, there is a critical minimum value, following an increase for higher amplitudes. Keulegan and Carpenter [7] found the critical KC number for a single cylinder to be KC ≈ 15. The results by Sarpkaya [8, 9] show a similar behavior at KC ≈ 13. In the present study, the smallest added mass coefficient for the five cylinder configuration is found when the amplitude of motion is $Z = 48\,\mathrm{mm}$, $Z = 50\,\mathrm{mm}$, $Z = 49\,\mathrm{mm}$, $Z = 49\,\mathrm{mm}$, and $Z = 48\,\mathrm{mm}$, for $T = 1.0\,\mathrm{s}$ to $T = 2.0\,\mathrm{s}$, respectively. This corresponds to a mean KC $= 5.1$, when normalizing with the diameter of one cylinder. The speed up due to the flow restriction, caused by the row of cylinders, is not reflected in this KC number. If a simple control volume analysis is applied, where the distance between the center of the two outermost cylinders is used as the total change in area compared with a one cylinder configuration, there is $4R$ unrestricted flow distance over a distance of $12R$. Consequently, the critical KC number could be expected to be of order $4R/12R = 1/3$ of the critical KC number for one cylinder, which is in reasonable agreement with the results for one cylinder (KC $\approx$ 13-15).

The drop in the added mass coefficient at the critical KC number is significant, but unlike the results by Sarpkaya [8] for one cylinder at similar β values, the added mass coefficient does not become negative in the present study. Here, the five periods of oscillations correspond to $1750 \leq \beta \leq 3500$, and the critical added mass is approximately 65 % of the numerical potential flow solver result, independent on the period of oscillation. On the other hand, the results for one cylinder by Sarpkaya [8]

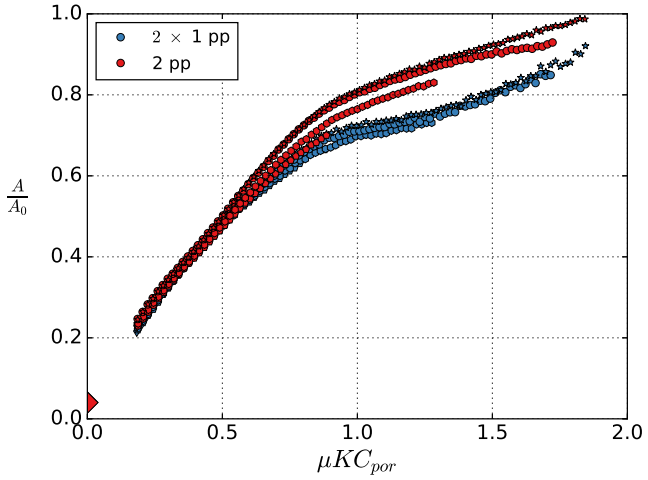

FIGURE 6. ADDED MASS OF TWO PARALLEL PLATES AND TWO TIMES ONE SINGLE PLATE. BEM RESULTS ARE ILLUSTRATED BY THE MARKERS AT ZERO AMPLITUDE.

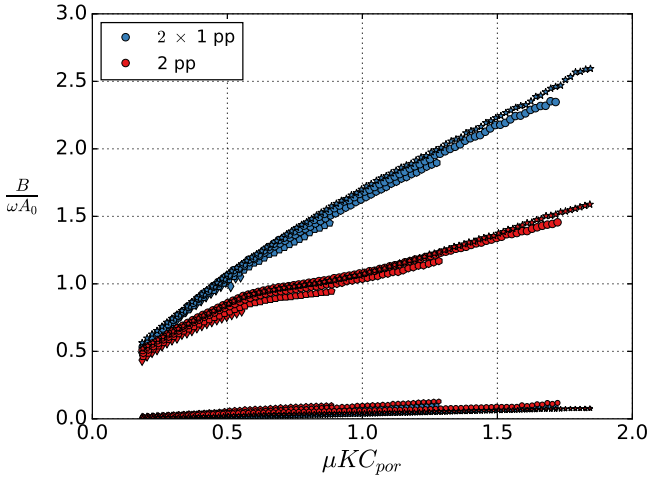

FIGURE 7. MEASURED DAMPING AND ESTIMATED WAVE RADIATION DAMPING OF TWO PARALLEL PLATES AND TWO TIMES ONE SINGLE PLATE.

yield critical added mass coefficients of -0.2, 0.3, and 0.6 for $\beta = 1985$, $\beta = 3123$, and $\beta = 4480$, when normalizing with the area of one cylinder. As has been pointed out by Singh [10], other studies have shown negligible β dependence or opposite trends to that found by Sarpkaya, with decreasing added mass coefficient when increasing β.

Normalized damping coefficients for configurations 1 and 2 are presented in Fig. 5 as functions of $\mu\mathrm{KC}_{\mathrm{por}}$. Additionally, the estimated wave radiation damping coefficients [3, pp. 45–47], based on the measured wave elevation of radiated waves downstream of the model rig, are given. The wave radiation damping results are indicated by the two curves in the very lowest part of the plot. Both configurations yield only small wave radiation damping contributions, with all values $\frac{B}{\omega A_0} < 0.05$. Wave reflection from the beaches may influence the force coefficients, and in general there may be temporal effects giving different loads for different oscillations within a series. However, the effect is found to be quite small for all tested configurations as previously pointed out and illustrated with error bars in Fig. 4.

The realistic protection structure results [2, 6] are between the results of configurations 1 and 2, but the general trend and values are closer to the results of the porous plate, which is likely a result of the numerous openings of the protection structure model. In addition to the structural differences between the ideal porous plate and the model scaled protection structure, the differences in test setup (near two-dimensional versus three-dimensional) will influence the added mass and damping coefficients.

Single versus two parallel plates

Results for configuration 3, two parallel porous plates with $P = 27.8\,\%$ and distance 120 mm (2 pp), are presented in Figs. 6 and 7. The coefficients for one porous plate (config. 1), multiplied by a factor 2, are given for comparison (2×1 pp). Normalization is, for consistency, made against the added mass of a single solid plate, A_0.

The added mass coefficients are nearly identical for $\mu\mathrm{KC}_{\mathrm{por}} \lesssim 0.8$. For higher amplitudes, the parallel plate case yields somewhat higher values than those found by multiplying the single plate coefficients by two, although the relative difference is within 15 %. Some period dependence is visible at high amplitudes. The DNV GL recommended practice values [4] are conservative compared to the experimental results. However, since the added mass coefficient of two plates in parallel is larger than two times one plate at high amplitudes, the values are closer than what is the case for one porous plate. The low KC relation, Eq. (12), yields 0.74 for two plates, which is in line with the experiments at moderate amplitudes, whereas the all KC relation of Eq. (13) yields 1.09, which is conservative for all tested amplitudes, but only approximately 10 % higher than the experimental values at the very highest amplitudes tested in the present study.

Normalized damping coefficients are presented in Fig. 7. The calculated wave radiation damping coefficients, are also included. As for configurations 1 and 2, the calculated wave radiation damping accounts for only a minor part of the total damping of configuration 3. The damping is in general significantly lower for two parallel plates than that for a single plate multiplied by two. For the highest amplitudes, the damping coefficients of two

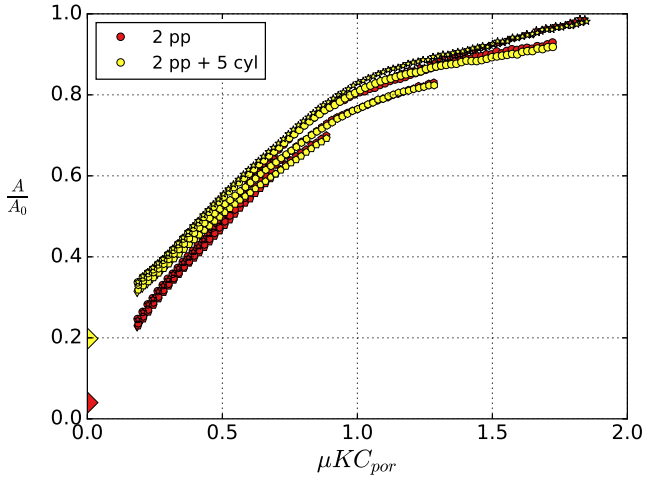

FIGURE 8. ADDED MASS OF TWO PARALLEL PLATES AND TWO PARALLEL PLATES WITH FIVE CYLINDERS IN BETWEEN. BEM RESULTS ARE ILLUSTRATED BY THE MARKERS AT ZERO AMPLITUDE.

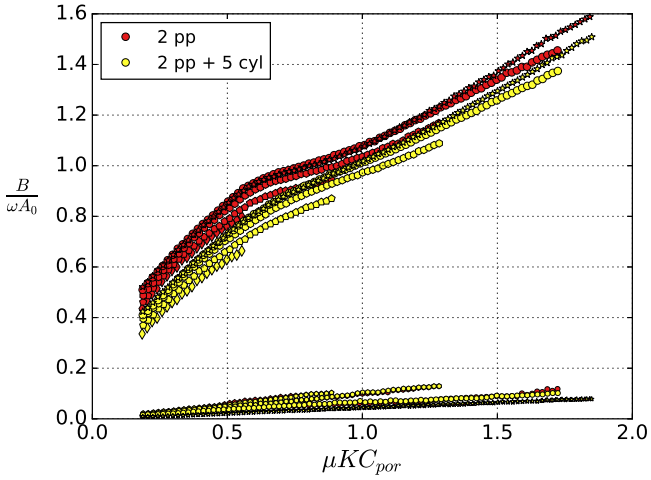

FIGURE 9. MEASURED DAMPING AND ESTIMATED WAVE RADIATION DAMPING OF TWO PARALLEL PLATES AND TWO PARALLEL PLATES WITH FIVE CYLINDERS IN BETWEEN.

parallel plates are closer to the results of one single plate than two times a single plate (compare with Fig. 5).

Parallel plates with in-line cylinders

Results for configuration 4, two porous plates with five cylinders in between (2 pp + 5 cyl), are presented in Figs. 8 and 9. Configuration 4 is here compared with the results for two porous parallel plates with the same distance, but without the cylinders in between, that is, configuration 3 (2 pp).

The added mass coefficients are presented in Fig. 8. BEM results are represented by the diamond markers at zero forcing amplitude. If the same extrapolation technique as previously described (linear using the three smallest amplitudes) is performed, the relative differences between the expected value and the BEM results are 32 % and 9 % for, respectively, config. 3 and 4. At small amplitudes, the five cylinders contribute to an increase in the added mass coefficient similarly as the increase found in the numerical potential flow solver solutions. However, the influence of the cylinders reduces with increasing amplitude, and is barely noticeable for $\mu\mathrm{KC}_{\mathrm{por}} > 0.5$. Here, the two configurations yield almost identical added mass coefficients. For the moderate and higher amplitudes of the present study, the added mass coefficients are found more sensitive to the period of oscillation than to the presence of the cylinders. For the case of two porous plates and five cylinders, the recommended practice values are conservative compared to the experiments. The low KC value, Eq. (12), 0.84 is significantly higher than what is found at small KC values in the experiments, but close to the experimental values at $\mu\mathrm{KC}_{\mathrm{por}} \approx 1$. Since the effect of the cylinders on the added mass at moderate and high amplitudes is negligible, the all KC value, Eq. (13), of 1.20 is more conservative than for configuration 3, and approximately 20 % higher than the experimental values at the very highest amplitudes in the present study.

Normalized damping coefficients are shown in Fig. 9. As for the other configurations, the wave radiation damping represents only a small part of the total damping force coefficients (lower part of the figure). The two parallel plates only configuration yields slightly higher damping coefficients than the configuration with cylinders in between. The strong resemblance of the curves indicates that the plates have a dominant contribution to damping. The reason why the presence of the five cylinders cause less damping is subject for further studies.

Importance of damping versus added mass

So far, hydrodynamic *coefficients* have been presented. However, it is the *force* which is ultimately the important quantity. The relative importance of the damping *force* compared to the added mass *force*, for all four configurations 1–4, is presented in Fig. 10.

In the literature and RP, the main focus has been given to added mass. For the presently tested porous plate, however, the damping force is dominating for all tested $\mu\mathrm{KC}_{\mathrm{por}}$, with typical values $\frac{B}{\omega A} \approx 2.5$. From the total force perspective of harmonic motions with only added mass and damping, a relation of 2.5 means that the damping force is responsible for 93 % of the total

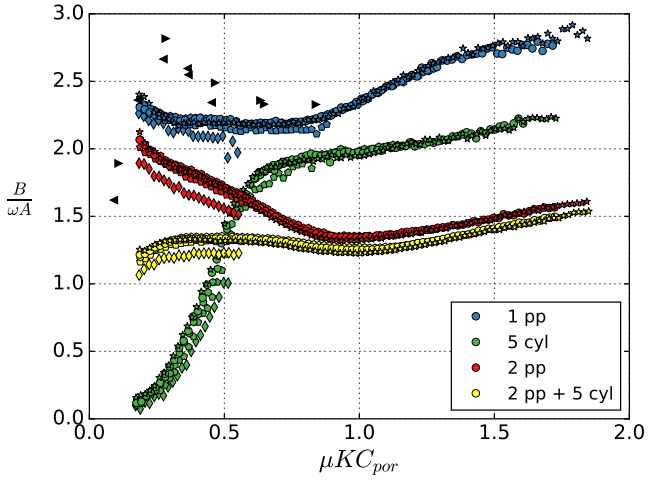

FIGURE 10. RATIO OF DAMPING AND ADDED MASS FORCE FOR THE FOUR CONFIGURATIONS. BLACK MARKERS ARE RESULTS FOR A SUBSEA PROTECTION STRUCTURE [2, 6].

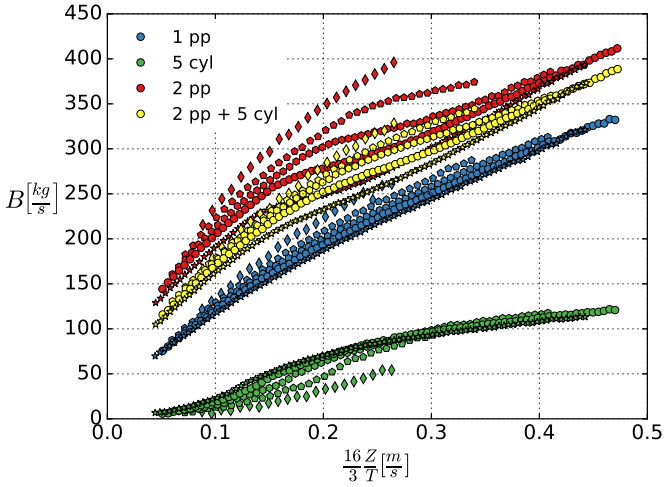

FIGURE 11. DAMPING OF THE FOUR CONFIGURATIONS PRESENTED WITHOUT NORMALIZATION AS FUNCTION OF THE EQUIVALENT VELOCITY.

hydrodynamic force amplitude $\left(\sqrt{\frac{2.5^2}{1^2+2.5^2}}\right)$, indicating the significance of the damping force. This has practical importance. A systematic study would indicate for what range of porosities this holds. An and Faltinsen [11] studied porous plates with 15.89 % and 7.945 % porosity, meaning roughly one-half and one-quarter of that presented in the present paper. For the 7.945 % porous plate, the added mass force and damping force are nearly equal, whereas for the 15.89 % porosity plate, the damping force dominates, being almost twice that of the added mass force. The trend is supported in the present study where the porosity is higher, $P = 27.8\,\%$, and the damping force dominates even more. An and Faltinsen emphasized the (unknown) contribution to damping from flow separation at the outer edges of the plate. Their study was three-dimensional, increasing the effect of plate-end flow separation. The significance of plate-end flow separation is subject for further studies.

The configuration with five cylinders has a regime of added mass dominance at small amplitudes, shifting towards damping dominance at larger amplitudes, similar to the known behavior of oscillating flow around a single cylinder [7]. The damping force dominates for the configuration with two parallel plates, although to a notable lesser extent than for a single porous plate. This has practical relevance, and is subject for further studies. For configuration 4, the significant added mass at low $\mu\mathrm{KC}_{\mathrm{por}}$, caused by the presence of the cylinders, yields a lower ratio of damping compared to the added mass. For the whole range of $\mu\mathrm{KC}_{\mathrm{por}}$ numbers, this configuration yields lower ratio than the parallel plates without cylinders, but for moderate and higher amplitudes the difference is marginal and typically within 5 %.

Damping as function of equivalent velocity

In Fig. 11, the damping coefficients without normalization are presented as function of the equivalent velocity, Eq. (10). Here, the damping coefficients of Eq. (9), B_1 and B_2, are recognized, respectively, as the extrapolated value at zero amplitude and the slope of the curve. The model may perhaps in practice be a reasonable model for a single porous plate, but is less descriptive for the other configurations. Significant period dependence is found when presenting the damping coefficients against the equivalent velocity. It is not obvious what B_1 and B_2 should be.

FINAL REMARKS

Brief discussions regarding experimental error sources, modeling of complex structures, as well as the use of damping model, are given in the following subsections.

Experimental errors

A considerable amount of work is invested to ensure the general quality of the experiments and analysis, including minimizing the effect from random and bias error sources. When calculating the hydrodynamic coefficients, the force difference between the experiments with and without the tested module is used. Ideally, the only difference in this net force estimation is the hydrodynamic force on the module, but the structural properties of the full model rig will be different than the empty model

rig, potentially influencing the force measurements. In addition to increasing the mass of oscillating rig, the models will increase the structural stiffness of the rig since they are fastened to the lower parts of the acrylic plates, thereby forcing a constant distance between the two plates, whereas the distance between the acrylic plates in the empty configuration depends on the fastening to the wooden box, at the top of the rig, only. Additionally, since the model rig is loosened and tightened between each configuration, there can be small differences in the experimental conditions. The distance between the acrylic glass end plates and the tank walls pose another challenge. Guiding plates and distance measuring are used when fasting the model rig, to ensure proper clearance, but some deviations in the placement and fastening of the model rig must be expected.

On the use of simplified scaled models

The tested structures are based on the characteristics of main members of actual subsea modules, but are in no way model scales of particular modules. The intention of the present study is to understand the loads on these, and to focus on the interaction of some characteristic shapes present in subsea modules. Obviously, there are differences in the flow around a cylinder and the flow around various subsea equipment. Similarly, an almost ideal porous plate consisting of a large number of holes will not possess an equivalent hydrodynamic behavior compared to a real subsea protection structure that may consist of rows of cylinders with gaps and openings in between.

For complex structures, the Reynolds number must be expected to be of important significance, in particular for models that have blunt shapes without fixed flow-separation points. It is therefore not obvious that models that look like realistic realizations of complex subsea structure will yield results that are closer to the full-scale structure, compared to more stylistic models that may capture the dominating hydrodynamic behavior. Consequently, the purpose of the experiments is to increase the understanding of the hydrodynamic loads on these type of structures, with emphasis on the fundamental hydrodynamics without losing too much generality, thus using ideal porous plates and cylinder elements is found useful in this respect.

Damping model

Even though the B_1 and B_2 model seemingly is fair for the porous plate, one should be careful using this type of model for small values of equivalent velocities, as the damping coefficient should converge towards zero at zero amplitude if there is no wave radiation. A behavior $B \propto \mathrm{KC}^{\frac{2}{3}}$, as discussed by Graham [12], may be relevant when the model has a flat plate type basic shape, but there is a lack of results at very small amplitudes in the present experiments, and the specific behavior can therefore not be confirmed. Nevertheless, for practical purposes at higher values of w_l, a model of B_1 and B_2 type seems reasonable for a single porous plate. The model can be relevant for more complex structures if the range of applicable equivalent velocities is limited, such that the values of B_1 and B_2 are close to constant, although one should note the non-negligible period dependence.

CONCLUSION

Four different 2D type configurations, relevant for subsea structures, were tested experimentally by forced oscillation tests for a large range of KC numbers and forcing periods. The present study shows, consistent with existing studies, that the hydrodynamic coefficients of simplified subsea structures, consisting of porous plate and cylinder members, are highly amplitude dependent. Significant interaction between different modules is demonstrated, and found to depend on the amplitude of motion, with increasing importance with increasing amplitude. The period dependence is in general small for all configurations. Interaction effects can give both increased and reduced force coefficients relative to superposition, depending on the distance between, and type of members, in a structure. In the case of two porous plates in parallel, the added mass coefficient was higher than superposition of two single plates, while the damping coefficient was lower. For the configuration of two plates with five cylinders in between, the added mass and damping coefficients were smaller than superposition of two parallel plates and five cylinders. Numerical potential flow results are found to agree well with extrapolation of the experimental results for the added mass in the low KC limit.

The recommended practice guidelines by DNV GL are found to yield conservative added mass coefficient estimates for the tested structures, particularly at small amplitudes of motions. The single porous plate results yield slightly higher hydrodynamic coefficients than the previous experiments of a subsea protection structure model, but the general behavior and amplitude dependence share strong similarities, supporting the use of porous plates as models for such subsea equipment.

An important aspect, not discussed earlier to our knowledge, is that the damping force dominates over the added mass force for most of the tested amplitudes and configurations.

ACKNOWLEDGEMENT

This work was financed by the Research Council of Norway, NFR project 237929 CRI MOVE.

REFERENCES

[1] Molin, B., 2011. "Hydrodynamic modeling of perforated structures". *Applied Ocean Research,* ***33***(1), pp. 1–11.

[2] Sandvik, P. C., Solaas, F., and Nielsen, F. G., 2006. "Hydrodynamic forces on ventilated structures". In Proceedings of

the International Offshore and Polar Engineering Conference, pp. 54–58.
[3] Faltinsen, O. M., 1993. *Sea Loads on Ships and Offshore Structures*. Cambridge Ocean Technology Series. Cambridge University Press.
[4] DNV GL AS. Modelling and analysis of marine operations. DNVGL-RP-N103 Edition July 2017. Obtained 2017-09-14.
[5] Sarkar, A., and Gudmestad, O. T., 2010. "Splash zone lifting analysis of subsea structures". In Proceedings of the International Conference on Offshore Mechanics and Arctic Engineering, Vol. 1, pp. 303–312.
[6] Sandvik, P. C., Solaas, F., and Firoozkoohi, R., 2016. "Hydrodynamic forces on complex subsea structures". In Marine Operations Special Symposium (MOSS 2016), Singapore.
[7] Keulegan, G. H., and Carpenter, L. H., 1958. "Forces on cylinders and plates in an oscillating fluid". *Journal of Research of the National Bureau of Standards,* ***60***(5), pp. 423–440.
[8] Sarpkaya, T., 1976. Vortex shedding and resistance in harmonic flow about smooth and rough circular cylinders at high reynolds numbers. Tech. rep., Monterey, California. Naval Postgraduate School.
[9] Sarpkaya, T., 1986. "Force on a circular cylinder in viscous oscillatory flow at low Keulegan–Carpenter numbers". *Journal of Fluid Mechanics,* ***165***, pp. 61–71.
[10] Singh, S., 1979. "Forces on bodies in an oscillatory flow". PhD thesis, Imperial College, University of London.
[11] An, S., and Faltinsen, O. M., 2013. "An experimental and numerical study of heave added mass and damping of horizontally submerged and perforated rectangular plates". *Journal of Fluids and Structures,* ***39***(Supplement C), pp. 87–101.
[12] Graham, J. M. R., 1980. "The forces on sharp-edged cylinders in oscillatory flow at low Keulegan–Carpenter numbers". *Journal of Fluid Mechanics,* ***97***(2), pp. 331–346.